Volume 24, No 3 | International Journal of Radiation Research, July 2026

Immunohistochemical double staining with TTF-1 and aldehyde fuchsin with CT scan enhances the detection of visceral pleural invasion in lung cancer

L. Wu*, Q. Lin, Y. Chen, N. Qiu, J. Huang

Department of Pathology, Fuzhou Pulmonary Hospital of Fujian, Fuzhou 350008, Fujian Province, China

► ***Original article***

Corresponding author:
Lianping Wu, M.D.,
E-mail: *wlpwcx1@163.com*

Received: August 2026
Final revised: August 2026
Accepted: August 2026

Int. J. Radiat. Res., July 2026; 24(3): 805-812

DOI: 10.61186/ijrr.24.3.30

Keywords: *Adenocarcinoma of lung, neoplasm invasiveness, immunohistochemistry, thyroid nuclear factor 1, tomography, X-ray computed.*

ABSTRACT

Background: Accurate assessment of visceral pleural invasion (VPI) is important for lung cancer staging and prognosis, but distinguishing PL0 from PL1 can be difficult on conventional histology. We evaluated whether combined thyroid transcription factor-1 (TTF-1) immunohistochemistry and aldehyde fuchsin elastic staining, interpreted with preoperative computed tomography (CT), facilitates VPI assessment in lung adenocarcinoma. ***Materials and Methods:*** This retrospective study included 76 patients with surgically resected lung adenocarcinoma. Clinicopathological characteristics, immunohistochemical findings, pathological stage, VPI status, CT features, and recurrence outcomes were reviewed. Selected sections underwent combined TTF-1/aldehyde fuchsin double staining. Principal component analysis (PCA) and Mahalanobis distance analysis were performed as exploratory analyses. ***Results:*** The mean age was 62.0 ± 8.8 years; 58.4% were female and 31.2% had a smoking history. EGFR mutations were detected in 58.4% of tumors. VPI was identified in 75 of 76 evaluable cases (98.7%). Double staining demonstrated the relationship of TTF-1-positive tumor cells to the visceral pleural elastic lamina, distinguishing the single PL0 case from PL1 lesions. Three patients (3.9%) developed recurrence 14–19 months after surgery. The first three principal components explained 64.5% of total variance; the PL0 case had the greatest Mahalanobis distance, whereas recurrent cases were not multivariate outliers. ***Conclusion:*** Combined TTF-1 and aldehyde fuchsin staining permits simultaneous visualization of tumor cells and the pleural elastic layer and may serve as a practical adjunct for distinguishing PL0 from PL1 in lung adenocarcinoma. CT may provide complementary information in integrated VPI assessment.

INTRODUCTION

Lung cancer remains the leading cause of cancer-related mortality worldwide, with approximately 2.5 million new cases diagnosed annually and China accounting for more than 40% of the global burden [1-3]. Despite advances in early detection and targeted therapy, outcomes after curative resection remain heterogeneous, underscoring the need for refined pathological risk stratification.

Among the histological determinants of aggressiveness in lung adenocarcinoma, visceral pleural invasion (VPI) - defined as tumor extension beyond the elastic layer of the visceral pleura (PL1) or onto the pleural surface (PL2) - carries particular staging and prognostic weight [4, 5]. Recognized as an independent adverse prognostic factor associated with nodal metastasis and reduced survival, VPI upstages otherwise T1 tumors to T2 in the TNM classification [6, 7]; however, its prognostic impact varies by radiological tumor type, with VPI conferring worse survival in pure-solid but not part-solid cT1-sized NSCLC [8]. Yet the distinction between tumor merely abutting the pleura (PL0) and true elastic layer invasion (PL1) can be remarkably subtle on routine sections, raising the question of whether conventional H&E staining alone is sufficient.

Elastic fiber stains such as elastica van Gieson and Victoria blue have long been used to highlight the pleural elastic lamina when H&E findings are equivocal [9]. These methods improve detection of transgression beyond the elastic layer, and dual-block elastic staining has been shown to increase VPI detection rates in large surgical series [10]. Elastic stains, however, delineate the connective tissue framework but do not identify tumor cells themselves, leaving the spatial relationship between neoplastic cells and the elastic lamina open to interpretation; this diagnostic uncertainty has driven interest in multimodal assessment, including CT-based prediction models [11, 12].

Thyroid transcription factor-1 (TTF-1) is a nuclear marker expressed in the majority of primary lung adenocarcinomas and is routinely used to confirm pulmonary origin [13, 14]. Combining TTF-1 immunohistochemistry with an elastic stain on a single slide would, in principle, allow simultaneous visualization of brown-stained tumor nuclei and the elastic fiber network, thereby clarifying whether tumor cells have actually crossed the pleural elastic

[DOI: 10.61186/ijrr.24.3.30]

layer [15]. Whether such a dual-staining approach, integrated with preoperative CT imaging, can reliably distinguish PL0 from PL1 in a consecutive surgical cohort has not been systematically evaluated.

In the present study, we evaluated the utility of combined TTF-1 immunohistochemistry and aldehyde fuchsin elastic staining, together with preoperative CT findings, for assessing VPI in 76 patients with surgically resected lung adenocarcinoma. The novelty of this work lies in the integrated imaging–pathology approach, in which tumor-cell identification and visualization of the visceral pleural elastic lamina are achieved simultaneously on the same histological section and interpreted alongside preoperative CT features. This approach is intended to clarify the spatial relationship between adenocarcinoma cells and the pleural elastic layer, particularly in diagnostically challenging PL0/PL1 cases in which conventional H&E assessment may be equivocal. In addition, we incorporated exploratory principal component analysis and Mahalanobis distance profiling to characterize the multivariate clinicopathological position of the PL0 case and patients who developed recurrence. Thus, the study extends previous work on elastic and immunohistochemical staining by examining its application within a multimodal framework combining histopathology, immunophenotyping, CT findings, and clinicopathological profiling.

MATERIALS AND METHODS

Study design and patient population

This is a retrospective observational study of patients with surgically resected primary lung adenocarcinoma who were treated at our tertiary referral facility during November 2023-December 2025. Consecutive patients were found from the institutional pathology database. Inclusion criteria were: histologically proven lung adenocarcinoma, availability of formalin-fixed paraffin-embedded (FFPE) tissue blocks for histological and immunohistochemical analyzes, complete clinicopathological data, and preoperative chest computed tomography (CT) imaging before surgery. Patients who received neoadjuvant chemotherapy or radiotherapy, had recurrent or metastatic tumors at diagnosis, or had insufficient tissue for further staining were excluded. In the present study, 76 patients who met the inclusion criteria were included. Demographic and clinicopathological data including age, sex, smoking history, tumor size, pathological stage, epidermal growth factor receptor (EGFR) mutation status, recurrence and follow-up results were collected from electronic medical records and pathology reports.

Histopathological evaluation

All surgical specimens were preserved in 10% formalin neutral buffered, routinely processed and embedded in paraffin. Tissue sections 4 micrometers thick were stained with hematoxylin and eosin (H&E) using normal laboratory methods. Histopathology was reviewed separately by two experienced pulmonary pathologists who were blinded to the radiological and clinical data. Attention was given to the contact of the tumor with the pleura, the intactness of the visceral pleural elastic layer and indications of pleural invasion. Visceral pleural invasion was classified using the criteria given by the International Association for the Study of Lung Cancer (IASLC) International Staging Committee [16]. Tumors that involved the lung parenchyma or extended to the pleural connective tissue without invasion of the elastic layer of the visceral pleura were classed as PL0. Tumors that extended beyond the elastic layer but not to the visceral pleural surface were classed as PL1, while tumors that extended to the visceral pleural surface were classified as PL2. Cases with uncertain pleural invasion by standard H&E staining were further evaluated by elastic staining and immunohistochemical staining.

Aldehyde fuchsin staining

To facilitate visualization of the visceral pleural elastic layer, aldehyde fuchsin staining was performed on representative tumor sections using a commercial elastic fiber staining kit (aldehyde fuchsin method), with all procedures conducted strictly in accordance with the kit instruction manual. Briefly, 4-μm formalin-fixed paraffin-embedded (FFPE) sections were deparaffinized in xylene and rehydrated through a graded ethanol series to distilled water; Lugol's iodine solution (Solution A) was then applied to fully cover the tissue sections and incubated for 10 minutes followed by rinsing under running tap water, after which sodium thiosulfate solution (Solution B) was added to cover the sections for 1–2 minutes of iodine removal and sections were rinsed again under running tap water before a brief rinse in 70% ethanol; thereafter, aldehyde fuchsin staining solution (Solution C) was dropped onto the sections to cover the entire tissue area, and sections were covered during incubation to prevent reagent evaporation and stained for 10–15 minutes at room temperature, then rinsed by immersion in 70% ethanol for 15 seconds followed by washing under running tap water, after which orange G staining solution (Solution D) was applied to cover the tissue for 1 second of counterstaining and sections were rinsed again under running tap water before being dehydrated through ascending ethanol gradients, cleared in xylene, and mounted with neutral balsam. Under light microscopy, elastic fibers of the visceral pleura were stained purplish red while the

[DOI: 10.61186/ijrr.24.3.30]

background connective tissue appeared pale yellow, enabling clear delineation of the pleural elastic lamina; the continuity and location of the elastic layer relative to the tumor front were evaluated microscopically, and the presence or absence of tumor extension beyond the elastic layer was recorded and correlated with other pathological and radiological findings.

Immunohistochemical analysis

Immunohistochemical staining was performed using an automated staining platform according to the manufacturers' recommendations. Sections were subjected to heat-induced antigen retrieval followed by incubation with primary antibodies against thyroid transcription factor-1 (TTF-1), Napsin A, and cytokeratin 7 (CK7). Antibody binding was detected using a polymer-based detection system with diaminobenzidine as the chromogen and hematoxylin counterstaining. TTF-1 expression was considered positive when distinct nuclear staining was observed in tumor cells. Napsin A and CK7 expression were assessed using established diagnostic criteria. Immunohistochemical findings were recorded as positive or negative.

Combined TTF-1 and aldehyde fuchsin double staining

To improve assessment of the tumor–pleura interface, selected tissue sections underwent combined TTF-1 immunohistochemistry and aldehyde fuchsin staining on the same slide. Briefly, after heat-induced antigen retrieval and incubation with the primary antibody against TTF-1, antibody binding was detected using a polymer-based detection system with diaminobenzidine (DAB) as the chromogen, yielding brown nuclear staining in tumor cells. Sections were then incubated in aldehyde fuchsin staining solution for 15–20 min at room temperature in a covered jar, differentiated in 95% ethanol, rinsed in running tap water, dehydrated, cleared in xylene, and mounted. This dual-staining technique enabled simultaneous visualization of adenocarcinoma cells and the visceral pleural elastic layer on a single slide. In the combined stain, TTF-1-positive tumor nuclei appeared brown, whereas elastic fibers of the visceral pleura were stained purplish red. The spatial relationship between tumor cells and the pleural elastic lamina was examined at high magnification. Cases were classified as PL1 when TTF-1-positive tumor cells were identified beyond the elastic layer demonstrated by aldehyde fuchsin staining. Conversely, cases were classified as PL0 when tumor cells remained adjacent to but did not penetrate an intact elastic layer. Representative photomicrographs were obtained for documentation and comparative analysis.

Computed tomography assessment

Preoperative chest CT scans were reviewed independently by two thoracic radiologists who were blinded to pathological findings. CT examinations were acquired using multidetector scanners with thin-section reconstruction ranging from 1 to 2 mm. Tumor size, location, pleural contact, pleural indentation, pleural thickening, and evidence of pleural surface involvement were assessed. Tumors demonstrating broad pleural attachment, pleural retraction, or irregular pleural thickening were considered radiologically suspicious for pleural invasion. Radiological findings were subsequently correlated with histopathological and double-staining results to determine the utility of integrated imaging-pathology assessment for detecting VPI.

Integrated evaluation of visceral pleural invasion

The final assessment of visceral pleural invasion was based on a comprehensive review of routine H&E sections, aldehyde fuchsin staining, combined TTF-1/aldehyde fuchsin double staining, and preoperative CT findings. Cases with discrepant findings among the different modalities were reviewed jointly by pathologists and radiologists until consensus was reached. Particular emphasis was placed on distinguishing PL0 from PL1 lesions, as identification of tumor extension beyond the visceral pleural elastic layer represents the key pathological criterion for VPI. The combined staining approach was used to clarify difficult cases in which the tumor–pleura interface could not be confidently interpreted on conventional histology alone.

Statistical analysis

Statistical analyses were performed using STATA (version MP17). Continuous variables were summarized as mean ± standard deviation (SD), whereas categorical variables were presented as frequencies and percentages. As an exploratory analysis, principal component analysis (PCA) was performed to evaluate the multivariate distribution of clinicopathological characteristics and identify observations occupying peripheral positions within the dataset. The analysis included age, sex, smoking history, Karnofsky Performance Status score, EGFR mutation status, EGFR subtype, visceral pleural invasion status, and pathological TNM stage. Variables were standardized prior to PCA. Principal component scores were generated from the first three principal components, which together explained 64.5% of the total variance. A Mahalanobis distance–based outlier score was subsequently calculated in the reduced principal component space, and patients were ranked according to their distance from the multivariate centroid. Recurrence-free survival was defined as the interval from surgical resection to documented recurrence or last follow-up. Statistical significance was defined as a two-sided P value of less than 0.05.

[DOI: 10.61186/ijrr.24.3.30]

RESULTS

Patient characteristics

A total of 76 patients were included in the study. The mean age was 62.0 ± 8.8 years, and 45 patients (58.4%) were female. Twenty-four patients (31.2%) had a history of smoking. The mean KPS score was 94.7 ± 6.0. EGFR mutations were identified in 45 patients (58.4%), including exon 19 deletion in 24 (32.9%), L858R mutation in 16 (21.9%), and other EGFR alterations in 1 patient (1.4%); 32 patients (41.6%) had EGFR wild-type tumors. Immunohistochemical analysis demonstrated TTF-1 positivity in 54 of 58 evaluable cases (93.1%), Napsin A positivity in 53 of 59 evaluable cases (89.8%), and CK7 positivity in all 64 tested cases (100%). Visceral pleural invasion was present in 75 of 76 evaluable patients (98.7%). The distribution of pathological TNM stages was as follows: IA1, 3 (4.0%); IA2, 25 (32.9%); IA3, 10 (13.2%); IB, 6 (7.9%); IIA, 8 (10.5%); IIB, 11 (14.5%); IIIA, 12 (15.8%); and IIIB, 1 (1.3%). Ki-67 expression was available for 17 patients and had a mean value of 34.2% ± 26.6%. During follow-up, disease recurrence occurred in 3 patients (3.9%).

Table 1. Baseline clinicopathological characteristics.

Characteristic	Value
Patients, n	76
Age, years	62.0 ± 8.8
Sex	
Male	32 (41.6%)
Female	45 (58.4%)
Smoking history	
Never smoker	53 (68.8%)
Ever smoker	24 (31.2%)
KPS score	94.7 ± 6.0
EGFR mutation	
Mutated	45 (58.4%)
Wild type	32 (41.6%)
EGFR subtype*	
Exon 19 deletion	24 (32.9%)
L858R	16 (21.9%)
Other mutation	1 (1.4%)
Wild type	32 (43.8%)
TTF-1 positive	54/58 (93.1%)
Napsin A positive	53/59 (89.8%)
CK7 positive	64/64 (100%)
Visceral pleural invasion present	75/76 (98.7%)
Pathological TNM stage	
IA1	3 (4.0%)
IA2	25 (32.9%)
IA3	10 (13.2%)
IB	6 (7.9%)
IIA	8 (10.5%)
IIB	11 (14.5%)
IIIA	12 (15.8%)
IIIB	1 (1.3%)
Ki-67, %†	34.2 ± 26.6
Recurrence (RFS event)	3 (3.9%)

Recurrence-free survival

Among the three patients who experienced recurrence, the total recurrence-free survival time at risk was 51 months. Recurrence occurred between 14 and 19 months after surgery, with a median recurrence-free survival of 18 months (interquartile range, 14-19 months), as shown in figure 1.

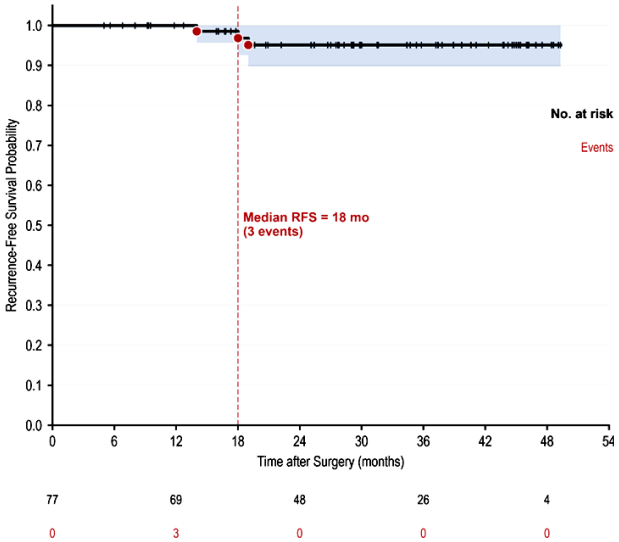

Figure 1. Kaplan–Meier analysis of recurrence-free survival (RFS) among 76 patients. The solid line represents the estimated RFS probability; shaded area denotes 95% confidence intervals. Three recurrences occurred at 14, 18, and 19 months (red circles); tick marks indicate censored observations. The number of patients at risk and the number of events are shown at 12-month intervals. Median RFS was 18 months (IQR, 14–19 months).

Principal component analysis

Principal component analysis (PCA) was performed to explore the multivariate structure of the clinicopathological dataset. The scree plot (figure 2A) showed that the first three principal components accounted for 64.5% of the total variance. The PCA biplot (figure 2B) illustrated the distribution of patients along PC1 and PC2 with variable loadings. Mahalanobis distance ranking across PC1–PC3 (figure 2C) identified the only patient without visceral pleural invasion (PL0) as the most extreme observation in the cohort (rank 1 among 71 evaluable patients). In contrast, the three patients who experienced recurrence did not demonstrate elevated outlier scores and ranked 33rd, 39th, and 51st, respectively.

Characteristics of the non-VPI (PL0) case

The sole patient without pleural invasion was a 62 -year-old male smoker with a KPS score of 90, EGFR wild-type adenocarcinoma, positive TTF-1, Napsin A, and CK7 expression, and pathological stage IA1 disease. No Ki-67 data were available for this patient. Compared with the VPI cohort, the non-VPI case was similar in age and immunophenotype but differed by being male, a smoker, EGFR wild type, and having the earliest pathological stage (table 2).

Histopathological assessment of visceral pleural invasion

Double staining with TTF-1

[DOI: 10.61186/ijrr.24.3.30]

immunohistochemistry and aldehyde fuchsin elastic stain facilitated clear delineation of the tumor–pleura interface. In the PL0 case (figure 3A), TTF-1–positive adenocarcinoma cells were observed in close proximity to the visceral pleura; however, the aldehyde fuchsin–stained elastic layer remained intact and was not traversed by tumor cells. Corresponding H&E staining (figure 3B) showed tumor near the pleural surface but no transgression of the elastic lamina, confirming the absence of visceral pleural invasion. In PL1 cases, double staining (Figure 3C, E) demonstrated TTF-1–positive tumor cells extending beyond the disrupted visceral pleural elastic layer, confirming VPI. H&E staining (figure 3D, F) showed adenocarcinoma infiltrating the subpleural connective tissue and visceral pleura, corroborating the double-staining findings.

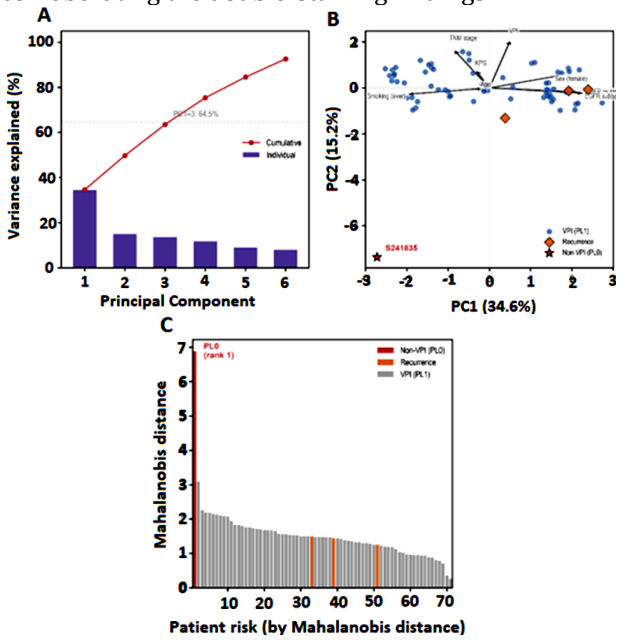

Figure 2. Principal component analysis (PCA) of 76 evaluable patients. **(A)** Scree plot showing the proportion of variance explained by each principal component; the first three components accounted for 64.5% of total variance. **(B)** PCA biplot of PC1 versus PC2; blue circles denote VPI-positive (PL1) patients, orange diamonds denote the three patients with recurrence, and the red star denotes the single PL0 patient (S241835). Arrows represent variable loadings. **(C)** Patients ranked by Mahalanobis distance from the multivariate centroid in PC1–PC3 space; the PL0 case had the highest distance (rank 1), whereas the three recurrent cases ranked 33rd, 39th, and 51st.

Integrated evaluation of visceral pleural invasion

Following integrated assessment of routine H&E sections, aldehyde fuchsin elastic staining, TTF-1/aldehyde fuchsin double staining, and preoperative CT findings, a final visceral pleural invasion status was established in 76 evaluable cases. Seventy-five cases (98.7%) were classified as PL1, whereas one case (1.3%) was classified as PL0. In the PL0 case, the integrated pathological assessment demonstrated TTF-1-positive adenocarcinoma cells adjacent to, but not extending beyond, an intact visceral pleural elastic lamina. In PL1 cases, tumor cells were identified beyond the elastic layer, confirming visceral pleural invasion.

Table 2. Comparison of the non-pleural invasion case and pleural invasion cases.

Characteristic	Non-Pleural Invasion (n=1)	Pleural Invasion (n=75)
Age, years	62	62.0 ± 8.9
Sex	Male	31 male (40.8%), 45 female (59.2%)
Smoking history	Ever smoker	23 (30.3%) ever smokers, 53 (69.7%) never smokers
KPS score	90	94.7 ± 6.0
EGFR mutation	Wild type	45 (59.2%) mutated, 31 (40.8%) wild type
EGFR subtype	Wild type	Exon 19 deletion 24 (33.3%), L858R 16 (22.2%), other mutation 1 (1.4%), wild type 31 (43.1%)
TTF-1 status	Positive	53/57 (93.0%) positive
Napsin A status	Positive	52/58 (89.7%) positive
CK7 status	Positive	63/63 (100%) positive
Pathological TNM stage	IA1	IA1 2 (2.7%), IA2 25 (33.3%), IA3 10 (13.3%), IB 6 (8.0%), IIA 8 (10.7%), IIB 11 (14.7%), IIIA 12 (16.0%), IIIB 1 (1.3%)
Ki-67, %	Not available	34.2 ± 26.6 (n=17)
Recurrence	No	3 (3.9%)

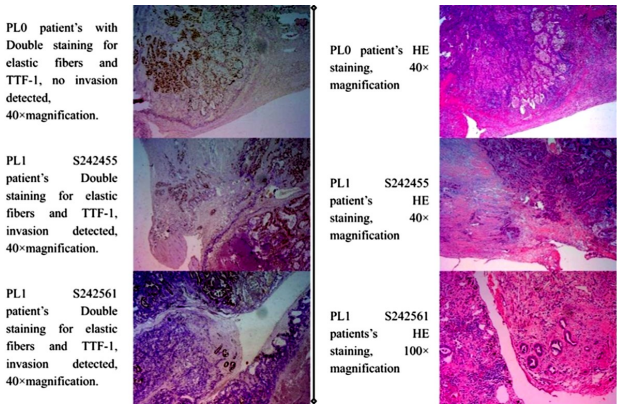

Figure 3. Histopathological assessment of visceral pleural invasion using TTF-1/aldehyde fuchsin double staining versus H&E staining. **(A)** PL0 case: double staining shows TTF-1-positive (brown) tumor cells adjacent to an intact aldehyde fuchsin-stained (purplish red) elastic layer; no tumor traversal is seen (40×). **(B)** Corresponding H&E staining of the PL0 case (40×). **(C)** PL1 case (patient S242455): double staining shows tumor cells breaching the elastic layer (40×). **(D)** Corresponding H&E staining of the same PL1 case (40×). **(E)** PL1 case (patient S242561): double staining demonstrates tumor extension beyond the disrupted elastic lamina (40×). **(F)** Corresponding H&E staining at higher magnification (100×).

Correlation of CT findings with histopathological assessment

We performed a case-matched analysis of preoperative CT findings and TTF-1/aldehyde fuchsin double-staining data for the typical PL0 and PL1 cases (figure 4, table 3). All three tumors were in touch with the visceral pleura, but the anatomical features of the tumor–pleura interface differed according to the eventual pathological VPI status.

[DOI: 10.61186/ijrr.24.3.30]

In the PL0 scenario (S241835) the lesion measured 0.9 cm (T1a) and had wide pleural contact on CT. The tumor–pleura interface was smooth without pleural depression or retraction and no accompanying pleural thickening. Therefore, the CT image was not suggestive for VPI. TTF-1/aldehyde fuchsin double stainings showed TTF-1 positive tumor cells near the border, but did not cross an intact continuous purplish-red pleural elastic lamina, supporting PL0.

Table 3. Case-matched correlation of preoperative CT findings with TTF-1/aldehyde fuchsin double-staining results in representative PL0 and PL1 lung adenocarcinomas.

Patient	Final VPI status	Tumor size on CT	Pleural contact	Pleural indentation/ retraction	Pleural thickening	CT impression of VPI	TTF-1/aldehyde fuchsin finding
S241835	PL0	0.9 cm (T1a)	Yes (broad abutment)	No (smooth interface)	No	Not suspicious	TTF-1-positive tumor cells adjacent to, but not crossing, an intact continuous purplish□red elastic lamina.
S242455	PL1	1.7 cm (T1b)	Yes (broad attachment)	Yes (focal, mild retraction)	Minimal (≤1 mm)	Suspicious	TTF-1-positive brown tumor nuclei extending beyond the disrupted pleural elastic lamina, confirming true elastic layer breach.
S242561	PL1	2.4 cm (T1c)	Yes (broad, linear contact)	Yes (prominent, V-shaped indentation)	Yes (focal, >1 mm)	Suspicious	TTF-1-positive tumor cells clearly traversing the fragmented purplish-red elastic fibers, with extension into the subpleural adipose tissue.

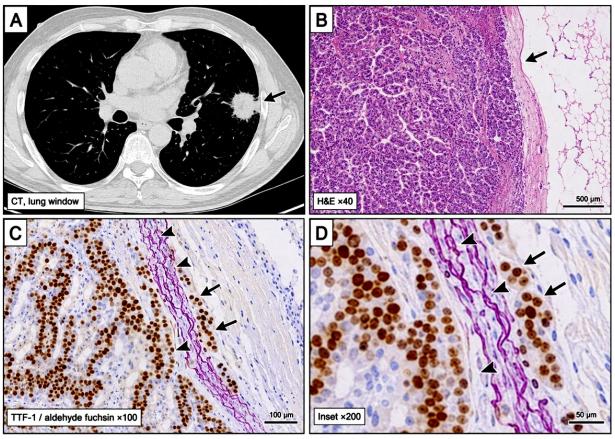

Figure 4. Integrated radiological-pathological correlation of visceral pleural invasion (PL1) in a representative lung adenocarcinoma case. **(A)** Preoperative axial chest CT scan (lung window) shows a peripheral solid nodule (arrow) with broad pleural contact and focal pleural indentation, raising radiological suspicion for visceral pleural invasion. **(B)** Corresponding H&E-stained section (×40) demonstrates the tumor mass adjacent to the visceral pleura; however, the elastic lamina is not distinctly visualized, rendering definitive assessment of elastic layer breach equivocal. **(C)** Combined TTF-1/aldehyde fuchsin double staining (×100) on the same lesion simultaneously highlights TTF-1-positive tumor cell nuclei (brown, arrowheads) and the visceral pleural elastic fibers (purplish red). Tumor cells are clearly identified extending beyond the disrupted elastic lamina (solid arrows), confirming PL1 invasion and illustrating the complementary value of preoperative CT imaging and dual histochemical/ immunohistochemical staining in comprehensive VPI assessment.

Conversely, both PL1 individuals had CT characteristics suggestive for pleural invasion. Patient S242455 had a 1.7-cm (T1b) tumor with extensive pleural adherence, isolated moderate pleural retraction, and limited pleural thickening (≤1 mm). On corresponding double labeling, TTF-1-positive brown tumor nuclei extended beyond the damaged pleural elastic lamina, demonstrating the invasion through the elastic layer. In patient S242561, the tumor was 2.4 cm (T1c) with extensive linear contact to the pleura, significant V-shaped pleural depression and focal pleural thickening >1 mm. Histopathological examination revealed that the TTF-1-positive tumor cells invaded into the fractured purple red elastic fibers and expanded into the subpleural adipose tissue, indicating PL1 invasion.

DISCUSSION

In this retrospective cohort of 76 surgically resected lung adenocarcinomas, VPI was identified in 75 of 76 evaluable cases (98.7%) with only one PL0 tumor. The tumor–pleura interface was clearly demarcated by combined TTF-1 immunohistochemistry and aldehyde fuchsin elastic staining. In the PL0 case, TTF-1–positive tumor cells bordered but did not penetrate an intact, uniformly stained elastic layer, while in PL1 cases brown-stained nuclei were observed beyond the disrupted purplish-red elastic lamina. Recurrence was observed in only 3 patients (3.9%) between 14 and 19 months after surgery, which reflects the mostly early-stage composition of the cohort. The first three principal components in the PCA explained 64.5% of the variation in eight clinicopathological variables, and the Mahalanobis distance ranking identified the single PL0 patient as the most extreme multivariate outlier (rank 1), while the three recurrent cases ranked 33rd, 39th and 51st, implying that they did not occupy a distinct peripheral position in the clinicopathological space.

Our results are in line with the growing evidence that dedicated elastic staining improves the detection of VPI over H&E alone. Liang *et al.* [17] in a series of 1,055 resected NSCLCs ≤3 cm showed that elastic staining improved the VPI detection by 13.7% and 8.2% for two independent pathologists and suggested that PL1 tumors ≤2 cm should be T1 rather than

[DOI: 10.61186/ijrr.24.3.30]

upstaged to T2. More recently, Yeh *et al.* [18] further refined the PL classification, demonstrating that tumor invasion through the external elastic lamina (PL-e), rather than invasion within the internal elastic lamina (PL-i), independently predicted worse disease-free and overall survival in pulmonary nonmucinous adenocarcinoma. These findings highlight the prognostic value of accurately localizing tumor cells in relation to the elastic framework. The prognostic and therapeutic significance of VPI has been quantified increasingly in large cohorts. Wang *et al*. [19] analyzed 87,045 SEER patients and developed a nomogram in which deeper pleural invasion (PL1/PL2) was an independent predictor of worse overall survival. Neri *et al*. [20] showed that on the biological level VPI and microscopic vessel invasion correlated with epithelial-mesenchymal transition and cancer stemness markers, providing a mechanistic basis for the aggressive behavior. Ozden *et al*. [21] observed graded survival differences between PL0, PL1 and PL2 (39.5 vs 35.1 vs 24.7 months) where PL2 was an independent negative prognostic factor, and Huang *et al*. [22] reported better outcomes for lobectomy compared to sublobar resection in stage IB peripheral NSCLC with VPI ≤3 cm in a propensity-score–matched SEER analysis. Ruan *et al*. [23] systematically reviewed the diagnosis, treatment and prognosis of stage IB NSCLC with VPI, and pointed out that accurate PL classification directly guides the selection of adjuvant therapy. Preoperative CT and advanced computational methods are continuously improving the noninvasive prediction of VPI. Lin *et al*. [24] developed a CT-based deep learning model to predict VPI and survival simultaneously in stage IA adenocarcinoma. Choi *et al.* [25] reported that a deep learning model achieved radiologist-level performance with adaptive sensitivity and specificity, whereas Kim *et al*. [26] showed that CT-defined VPI had limited independent prognostic value in T1 disease despite moderate diagnostic accuracy. Kudo *et al*. [27] demonstrated that an AI algorithm on high-resolution CT reached 76.4% sensitivity for VPI detection in stage I NSCLC. Beyond deep learning, Na *et al*. [28] showed that pleural carcinoembryonic antigen levels and maximum standardized uptake value on PET-CT predicted VPI in cT1N0M0 disease, and radiomics-based nomograms integrating intratumoral and peritumoral CT features have achieved AUCs of 0.85-0.89 for VPI prediction in part-solid and solid adenocarcinomas [29, 30]. A recent narrative review [31] synthesized these advances and emphasized the complementary roles of imaging, histopathology, and molecular markers in multimodal VPI assessment. The present study extends this literature by integrating TTF-1/aldehyde fuchsin double staining with preoperative CT, recurrence outcomes, and multivariate PCA-based profiling in a consecutive surgical cohort.

Several limitations should be acknowledged. First, the cohort was highly imbalanced, with only one PL0 case among 76 evaluable patients, which precluded formal statistical comparison between PL0 and PL1 groups and limited assessment of diagnostic accuracy. Second, the small number of recurrence events (n = 3) precluded robust survival analysis or identification of independent prognostic factors; the censored observations in the Kaplan–Meier analysis further reflect limited follow-up for some patients. Third, the single-center, retrospective design carries inherent selection bias. Finally, although PCA provided an unbiased multivariate overview, the sample size of 71 evaluable patients limited the stability of the component structure. Larger, prospective, multicenter studies with balanced PL0/PL1 representation and longer follow-up are needed to validate these findings.

CONCLUSION

Combined TTF-1 immunohistochemistry and aldehyde fuchsin elastic staining provides clear, simultaneous visualization of tumor cells and the visceral pleural elastic layer, facilitating reliable distinction between PL0 and PL1 in surgically resected lung adenocarcinoma. Integration with preoperative CT and multivariate clinicopathological profiling further supports comprehensive VPI assessment. Despite the predominance of VPI-positive cases limiting statistical power, this dual-staining approach represents a practical adjunct for routine pathological evaluation, particularly in diagnostically challenging specimens.

Acknowledgments: We thank all colleagues in the Department of Pathology for their support.

Ethics Approval: This study was approved by the Ethics Committee of **Fuzhou Pulmonary Hospital of Fujian** (Approval No.: 2023-010(Research)-02).

Conflicts of interest: The authors declare no conflicts of interest.

Funding: None.

Authors' contributions: L.W. and Q.L., conceived and designed the study. Y.C. and N.Q., performed the data collection and statistical analysis. J.H. drafted the manuscript. L.W. and Q.L., critically revised the manuscript for important intellectual content. All authors reviewed and approved the final version of the manuscript and agree to be accountable for all aspects of this work.

Data availability statement: The datasets used and analyzed during the current study are available from the corresponding author upon reasonable request.

Declaration of AI use: Artificial intelligence (AI) tools were used solely for language improvement, including refinement of grammar, clarity, readability, and academic style. AI was not used for study design, data analysis, interpretation of results, generation of

[DOI: 10.61186/ijrr.24.3.30]

scientific content, or preparation of figures or data. All manuscript content was reviewed and approved by the authors, who take full responsibility for the final work.

REFERENCES

1. Guo L, Zhu C, Cai L, *et al.* (2024) Global burden of lung cancer in 2022 and projected burden in 2050. *Chin Med J (Engl),* ***137****(21): 2576-2582*.
2. Filho AM, Laversanne M, Ferlay J, *et al.* (2025) The GLOBOCAN 2022 cancer estimates: Data sources, methods, and a snapshot of the cancer burden worldwide. *Int J Cancer,* ***156****(7): 1336-1346*.
3. Ji Y, Zhang Y, Liu S, *et al.* (2025) The epidemiological landscape of lung cancer: current status, temporal trend and future projections based on the latest estimates from GLOBOCAN 2022. *J Natl Cancer Cent,* ***5****(3): 278-283*.
4. Nicholson AG, Tsao MS, Beasley MB, *et al.* (2022) The 2021 WHO classification of lung tumors: Impact of advances since 2015. *J Thorac Oncol,* ***17****(3): 362-384*.
5. Minamino F, Araujo P, Dambrosio P, *et al.* (2024) The association of visceral pleural invasion with skip N2 metastasis on clinical stage IA NSCLC. *Clinics,* ***79****: 100334*.
6. Wightman SC, Lee JY, Ding L, *et al.* (2022) Adjuvant chemotherapy for visceral pleural invasion in 3-4-cm non-small-cell lung cancer improves survival. *Eur J Cardiothorac Surg,* ***62****(1): ezab498*.
7. Rami-Porta R and Eberhardt WEE (2018) Clinical implications of the innovations in the primary tumour and metastasis of the 8th edition of the TNM classification for lung cancer. *J Thorac Dis,* ***10*** *(Suppl 22): S2682-S2685*.
8. Okada S, Hattori A, Matsunaga T, *et al.* (2021) Prognostic value of visceral pleural invasion in pure-solid and part-solid lung cancer patients. *Gen Thorac Cardiovasc Surg,* ***69****(2): 303-310*.
9. Xie LW and Wang J (2021) Evaluating three elastic-fiber staining methods for detecting visceral pleural invasion in lung adenocarcinoma patients. *Clin Lab,* ***67****(7): 1570-1575*.
10. Li S, Huang Y, Zhang L, *et al.* (2023) Clinical significance of dual-block elastic stain evaluating visceral pleural invasion in peripheral non-small cell lung cancer. *Int J Surg Pathol,* ***31****(2): 175-183*.
11. Onoda H, Higashi M, Murakami T, *et al.* (2021) Correlation between pleural tags on CT and visceral pleural invasion of peripheral lung cancer that does not appear touching the pleural surface. *Eur Radiol,* ***31****(12): 9022-9029*.
12. Shi J, Li F, Yang F, *et al.* (2021) The combination of computed tomography features and circulating tumor cells increases the surgical prediction of visceral pleural invasion in clinical T1N0M0 lung adenocarcinoma. *Transl Lung Cancer Res,* ***10****(11): 4266-4280*.
13. Nakra T, Singh V, Nambirajan A, *et al.* (2021) Correlation of TTF-1 immunoexpression and EGFR mutation spectrum in non-small cell lung carcinoma. *J Pathol Transl Med,* ***55****(4): 279-288*.
14. Guan L, Zhao X, Tang L, *et al.* (2021) Thyroid Transcription Factor-1: Structure, Expression, Function and Its Relationship with Disease. *Biomed Res Int,* ***2021****: 9957209*.
15. Shen G, Dong J, Xiang Z, *et al.* (2022) Double staining of elastic fibre and immunohistochemistry is helpful to differentiate pleural invasion of lung cancer. *J Clin Pathol,* ***75****(3): 215-216*.
16. Travis WD, Brambilla E, Rami-Porta R, *et al.* (2008) Visceral pleural invasion: pathologic criteria and use of elastic stains: proposal for the 7th edition of the TNM classification for lung cancer. *J Thorac Oncol,* ***3****(12): 1384-1390*.
17. Liang RB, Li P, Li BT, *et al.* (2021) Modification of pathologic T classification for non-small cell lung cancer with visceral pleural invasion: data from 1,055 cases of cancers ≤3 cm. *Chest,* ***160****(2): 754-764*.
18. Yeh YC, Chiang CH, Hsu PK, *et al.* (2025) Tumor cell invasion of the external elastic lamina designates visceral pleural invasion and predicts poorer patient outcomes in pulmonary nonmucinous invasive adenocarcinoma. *J Thorac Oncol,* ***20****(12): 1791-1800*.
19. Wang F, Li P, Li F (2021) Nomogram for predicting the relationship between the extent of visceral pleural invasion and survival in non-small-cell lung cancer. *Can Respir J,* ***2021****: 8816860*.
20. Neri S, Menju T, Sowa T, *et al.* (2019) Prognostic impact of microscopic vessel invasion and visceral pleural invasion and their correlations with epithelial-mesenchymal transition, cancer stemness, and treatment failure in lung adenocarcinoma. *Lung Cancer,* ***128****: 13-19*.
21. Ozden S, Gokdemir I, Kiyik M (2024) The relationship between the degree of visceral pleural invasion and survival in non-small cell lung cancer. *North Clin Istanb,* ***11****(5): 367-372*.
22. Huang W, Deng HY, Lin MY, *et al.* (2022) Treatment modality for stage IB peripheral non-small cell lung cancer with visceral pleural invasion and ≤3 cm. *Front Oncol,* ***12****: 830470*.
23. Ruan Z, Zhuo X, Xu C (2024) Diagnosis, treatment, and prognosis of stage IB non-small cell lung cancer with visceral pleural invasion. *Front Oncol,* ***13****: 1310471*.
24. Lin X, Liu K, Li K, *et al.* (2024) A CT-based deep learning model: visceral pleural invasion and survival prediction in clinical stage IA lung adenocarcinoma. *iScience,* ***27****(1): 108712*.
25. Choi H, Kim H, Hong W, *et al.* (2021) Prediction of visceral pleural invasion in lung cancer on CT: deep learning model achieves a radiologist-level performance with adaptive sensitivity and specificity to clinical needs. *Eur Radiol,* ***31****(5): 2866-2876*.
26. Kim H, Goo JM, Kim YT, *et al.* (2019) CT-defined visceral pleural invasion in T1 lung adenocarcinoma: lack of relationship to disease-free survival. *Radiology,* ***293****(3): 741-749*.
27. Kudo Y, Saito A, Horiuchi T, *et al.* (2025) Preoperative evaluation of visceral pleural invasion in peripheral lung cancer utilizing deep learning technology. *Surg Today,* ***55****(1): 18-28*.
28. Na HR, Moon SW, Kim KS, *et al.* (2024) Pleural carcinoembryonic antigen and maximum standardized uptake value as predictive indicators of visceral pleural invasion in clinical T1N0M0 lung adenocarcinoma. *J Chest Surg,* ***57****(1): 44-52*.
29. Wang F, Pan X, Zhang T, *et al.* (2024) Predicting visceral pleural invasion in lung adenocarcinoma presenting as part-solid density utilizing a nomogram model combined with radiomics and clinical features. *Thorac Cancer,* ***15****(1): 23-34*.
30. Zha X, Liu Y, Ping X, *et al.* (2022) A nomogram combined radiomics and clinical features as imaging biomarkers for prediction of visceral pleural invasion in lung adenocarcinoma. *Front Oncol,* ***12****: 876264*.
31. Wang Y, Lyu D, Fan L, *et al.* (2024) Research progress in predicting visceral pleural invasion of lung cancer: a narrative review. *Transl Cancer Res,* ***13****(1): 462-470*.

[DOI: 10.61186/ijrr.24.3.30]